PHYSICAL REVIEW C **77**, 054313 (2008)

Three-body structure of low-lying ^{12}Be states

C. Romero-Redondo and E. Garrido
Instituto de Estructura de la Materia, CSIC, Serrano 123, E-28006 Madrid, Spain

D. V. Fedorov and A. S. Jensen
Department of Physics and Astronomy, University of Aarhus, DK-8000 Aarhus C, Denmark
(Received 5 December 2007; published 22 May 2008)

We investigate to what extent a description of ^{12}Be as a three-body system made of an inert ^{10}Be core and two neutrons is able to reproduce the experimental ^{12}Be data. Three-body wave functions are obtained with the hyperspherical adiabatic expansion method. We study the discrete spectrum of ^{12}Be, the structure of the different states, the predominant transition strengths, and the continuum energy spectrum after high-energy fragmentation on a light target. Two 0^+, one 2^+, one 1^-, and one 0^- bound states are found; the first four are known experimentally, whereas the 0^- is predicted as an isomeric state. An effective neutron charge, reproducing the measured $B(E1)$ transition and the charge rms radius in ^{11}Be, leads to a computed $B(E1)$ transition strength for ^{12}Be in agreement with the experimental value. For the $E0$ and $E2$ transitions, the contributions from core excitations could be more significant. The experimental ^{10}Be-neutron continuum energy spectrum is also well reproduced, except in the energy region corresponding to the $3/2^-$ resonance in ^{11}Be where core excitations contribute.

DOI: 10.1103/PhysRevC.77.054313 PACS number(s): 21.45.−v, 21.60.Gx, 31.15.xj, 27.20.+n

I. INTRODUCTION

The second lightest bound nucleus in the $N = 8$ isotonic chain is ^{12}Be, placed in the nuclear chart just above the widely investigated Borromean ^{11}Li nucleus. These two nuclei are essential to understand the breakdown of the $N = 8$ shell closure when the dripline is approached. The parity inversion in ^{11}Be, known since the early 1970s [1], is a clear indication of this fact. The particle unstable nucleus ^{10}Li should in principle have the same neutron configuration as ^{11}Be. Several theoretical works also predicted the existence of an intruder low-lying s-wave state [2–4]. The available experimental data concerning the ground state properties of ^{10}Li are, however, controversial, although most of them point toward the existence of such a low-lying virtual s state [5–8]. This result has been confirmed in recent work [9].

These properties of ^{11}Be and ^{10}Li clearly suggest that the p-sd shell gap is reduced when approaching the neutron dripline, leading to a structure of ^{12}Be and ^{11}Li with a large contribution from sd configurations. This has been confirmed theoretically and experimentally for both ^{12}Be [10–13] and ^{11}Li [4,14,15].

The ^{11}Li properties have been successfully described by the use of three-body models that freeze the degrees of freedom of the ^{9}Li core [16,17]. It is then tempting to follow a similar procedure to investigate ^{12}Be. In fact, although ^{12}Be is not Borromean, ^{11}Be is considered to be the prototype of one-neutron halo nuclei [18–20], and therefore a description of ^{12}Be as a ^{10}Be core surrounded by two neutrons appears to be a good first approach.

An important advantage of ^{12}Be over ^{11}Li is that the properties of ^{11}Be are much better known than the ones of ^{10}Li, and therefore the uncertainties arising from the core-neutron interaction should in principle be smaller. However, while in ^{11}Li the ^{9}Li core is spherical, the ^{10}Be core in ^{12}Be is deformed, and this is one of the essential reasons for the shell closure's breaking in ^{12}Be. The ground state in ^{11}Be contains an important contribution from core-excited configurations [21]. Different theoretical calculations have estimated this contribution, and the results range from 40% in Ref. [22] to 10% in Refs. [23,24], passing through 20% in Refs. [25,26]. Recent experimental data [27,28] are consistent with a 16% admixture of core excitation in the ^{11}Be ground state wave function.

As a consequence of this, a description of ^{12}Be as an inert core surrounded by two neutrons is quite questionable, and the role played by the core excitations is an important issue to be clarified. In Ref. [29], a hyperspherical expansion of the three-body wave function was used to obtain the ground state of ^{12}Be including core excitations. It was found that simultaneous fitting of the experimental ground state energy and the experimental longitudinal momentum distribution of ^{10}Be after high-energy fragmentation of ^{12}Be required a strong core-excited component in the wave function ($\approx$42%).

However, after publication of that work, additional experimental information about the spectrum of ^{12}Be became available. A bound 2^+ state and a bound 1^- state were found with excitation energies of 2.10 [30,31] and 2.68 MeV [32], respectively. Also, the existence of a second 0^+ bound state with excitation energy of 2.24 MeV was already envisaged [33] (and later confirmed [34]). Also, the (^{12}Be,^{11}Beγ) one neutron removal measurements at the National Superconducting Cyclotron Laboratory (NSCL) at Michigan State University [12] allowed a direct estimate of the $\langle ^{11}\mathrm{Be}(j^\pi)|^{12}\mathrm{Be(gs)}\rangle$ spectroscopic factors. All these new data led the authors of Ref. [29] to review their calculations [35]. They found that a reasonable simultaneous matching of the data required a significant reduction of the core deformation, and hence a smaller contribution from core excitation ($\approx$20%).

Very recently, new experimental data on ^{12}Be have been provided [13]. Especially interesting is the continuum relative energy spectrum for ^{10}Be+n after high-energy breakup of ^{12}Be on a carbon target. This invariant mass spectrum is known to be very sensitive to the final state interaction [36,37] and, therefore, in our case, to the properties of the unbound ^{11}Be states. A reliable calculation of the spectrum requires inclusion of the ^{10}Be-neutron continuum states together with core-neutron resonances. This energy spectrum is then a very useful observable for investigating the role played by the ^{10}Be-neutron interaction and for constraining the remaining uncertainties in the structure of ^{12}Be.

In previous ^{12}Be three-body calculations (^{10}Be+n+n) [4,29,35], the wave functions were obtained using the hyperharmonic expansion. The employed neutron-core potentials were chosen to reproduce the bound ^{11}Be states and perhaps the first resonance at 1.78 MeV (excitation energy), but higher unbound states were ignored. This method is not the most efficient for a non-Borromean system such as ^{12}Be, where two of the two-body subsystems have bound states. This is because an infinite hyperharmonic basis is in principle needed to reproduce the correct two-body asymptotics [38]. The convergence of the hyperharmonic expansion is slow, and in practice the energies and rms radii are obtained after extrapolation of the numerical results [4,29,35] where the basis is progressively increased up to a maximum value of the hypermomentum $K_{\max} = 20$ for the ground state, and $K_{\max} = 12$ for the excited states.

In the present context, the hyperspheric adiabatic expansion method [39] is more appropriate. This method solves the Faddeev equations in coordinate space, treating symmetrically the three two-body interactions such that each of them only appears in its natural coordinates. This makes the method specially suitable for non-Borromean systems such as ^{12}Be, where more than one two-body subsystem has bound states. Also, the method permits the use of much larger values of the hypermomentum quantum number, which guaranties convergence of the results.

The main goal of the present work is to assess to what extent a three-body model with an inert ^{10}Be core is able to reproduce the existing rather large amount of both old and new experimental data concerning ^{12}Be, i.e., the ^{12}Be spectrum, the $E1$ and $E2$ transition strengths [31,32,40], the $\mathcal{M}(E0)$ [40], and the measured invariant mass spectrum [13]. The two-body potentials to be used in the calculations are fitted to reproduce the available two-body experimental data, in particular, the ^{11}Be data. In this sense, although the ^{10}Be core is considered an inert particle with spin and parity 0^+, the employed two-body interactions phenomenologically account for all effects of core excitation appearing in the corresponding channel. In particular, it is interesting to know if the weakly bound excited states can be understood as halo states and perhaps can be better described in a three-body model than the relatively well bound ground state. Relations between various quantities can be tested and new properties predicted. For this the hyperspheric adiabatic expansion method is well suited. By comparing computed results and available data, we can establish how large the contributions must be from the inclusion of core excitations.

The paper is organized as follows. In Sec. II we very briefly describe the basis of the three-body method. The different two-body interactions used in the calculations are detailed in Sec. III. The results are shown in Secs. IV, V, and VI, where we discuss the spectrum and structure of ^{12}Be, the electromagnetic transition strengths, and the invariant mass spectrum after high-energy breakup, respectively. We finish in Sec. VII with a summary and the conclusions. In the appendix some remarks about the $E1$ and $E2$ operators are given.

II. THEORETICAL FORMULATION

We assume ^{12}Be can be described as a three-body system made by a ^{10}Be core and two neutrons. The wave functions for the different bound states are obtained with the hyperspherical adiabatic expansion method. A detailed description of the method can be found in Ref. [39].

This method solves the Faddeev equations in coordinate space. The wave functions are computed as a sum of three Faddeev components $\psi^{(i)}(\boldsymbol{x}_i, \boldsymbol{y}_i)\,(i = 1, 2, 3)$, each of them expressed in one of the three possible sets of Jacobi coordinates $\{\boldsymbol{x}_i, \boldsymbol{y}_i\}$. Each component is then expanded in terms of a complete set of angular functions $\{\phi_n^{(i)}\}$

$$\psi^{(i)} = \frac{1}{\rho^{5/2}} \sum_n f_n(\rho)\phi_n^{(i)}(\rho, \Omega_i); \quad \Omega_i \equiv \{\alpha_i, \Omega_{x_i}, \Omega_{y_i}\}, \quad (1)$$

where $\rho = \sqrt{x^2 + y^2}$, $\alpha_i = \arctan(x_i/y_i)$, and Ω_{x_i} and Ω_{y_i} are the angles defining the directions of $\boldsymbol{x}_i$ and $\boldsymbol{y}_i$. Writing the Faddeev equations in terms of these coordinates, they can be separated into angular and radial parts:

$$\hat{\Lambda}^2\phi_n^{(i)} + \frac{2m\rho^2}{\hbar^2} V_{jk}(x_i)\left(\phi_n^{(i)} + \phi_n^{(j)} + \phi_n^{(k)}\right) = \lambda_n(\rho)\phi_n^{(i)}, \quad (2)$$

$$\left[-\frac{d^2}{d\rho^2} + \frac{2m}{\hbar^2}(V_{3b}(\rho) - E) + \frac{1}{\rho^2}\left(\lambda_n(\rho) + \frac{15}{4}\right)\right] f_n(\rho) + \sum_{n'}\left(-2P_{nn'}\frac{d}{d\rho} - Q_{nn'}\right) f_{n'}(\rho) = 0, \quad (3)$$

where V_{jk} is the two-body interaction between particles j and k, $\hat{\Lambda}^2$ is the hyperangular operator [39], and m is the normalization mass. In Eq. (3), E is the three-body energy, and the coupling functions $P_{nn'}$ and $Q_{nn'}$ are given, for instance, in Ref. [39]. The potential $V_{3b}(\rho)$ is used for fine tuning to take into account all those effects that go beyond the two-body interactions. In the present cases, it is rather small; and unless the opposite is explicitly said, this three-body potential is taken equal to zero.

It is important to note that the angular functions used in the expansion (1) are precisely the eigenfunctions of the angular part of the Faddeev equations. Each of them is in practice obtained by expansion in terms of the hyperspherical harmonics. Obviously this infinite expansion has to be cut off at some point, maintaining only the contributing components.

The eigenvalues $\lambda_n(\rho)$ in Eq. (2) enter in the radial equations (3) as a basic ingredient in the effective radial potentials. Accurate calculation of the λ eigenvalues requires,

for each particular component, a sufficiently large number of hyperspherical harmonics. In other words, the maximum value of the hypermomentum ($K_{\max}$) for each component must be large enough to ensure convergence of the λ functions in the region of ρ values where the $f_n(\rho)$ wave functions are not negligible.

Finally, the last convergence to take into account is the one corresponding to the expansion in Eq. (1). Typically, for bound states, this expansion converges rather fast, and usually three or four adiabatic terms are already sufficient.

III. TWO-BODY INTERACTIONS

It is known that for weakly bound systems, as for instance ^{6}He or ^{11}Li, the short distance behavior of the two-body potentials is relatively unimportant as long as they reproduce the low-energy scattering data. Then the essential three-body properties can be described [16].

A. Neutron-neutron potential

For the neutron-neutron interaction, we use a simple potential reproducing the experimental s- and p-wave nucleon-nucleon scattering lengths and effective ranges. It contains central, spin-orbit ($\boldsymbol{\ell}\cdot\boldsymbol{s}$), tensor ($S_{12}$), and spin-spin ($\boldsymbol{s}_1\cdot\boldsymbol{s}_2$) interactions, and is explicitly given as [41]

$$V_{nn}(r) = 37.05e^{(-(r/1.31)^2)} - 7.38e^{(-(r/1.84)^2)} - 23.77e^{(-(r/1.45)^2)}\boldsymbol{\ell}\cdot\boldsymbol{s} + (49.40e^{(-(r/1.31)^2)} + 29.53e^{(-(r/1.84)^2)})\boldsymbol{s}_1\cdot\boldsymbol{s}_2 + 7.16e^{(-(r/2.43)^2)}S_{12}, \quad (4)$$

where $\boldsymbol{\ell}$ is the relative orbital angular momentum between the two neutrons, and $\boldsymbol{s} = \boldsymbol{s}_1 + \boldsymbol{s}_2$ is the total spin. The strengths are in MeV and the ranges in fm. We will refer to this potential as the Gaussian neutron-neutron potential.

To test the role played by the short-distance properties of the neutron-neutron interaction, for some specific cases, we are also using the more sophisticated v_8 version of the nucleon-nucleon Argonne potential [42]. This is a nonrelativistic potential reproducing proton-proton and neutron-proton scattering data for energies from 0 to 350 MeV, neutron-neutron low-energy scattering data, as well as the deuteron properties.

B. Neutron-^{10}Be potential

For the neutron-core interaction, we have constructed an ℓ-dependent potential of the form:

$$V^{(\ell)}(r) = V_c^{(\ell)}(r) + V_{\rm so}^{(\ell)}(r)\boldsymbol{\ell}\cdot\boldsymbol{s}_n, \quad (5)$$

where $\boldsymbol{\ell}$ is the neutron-core relative orbital angular momentum and $\boldsymbol{s}_n$ is the spin of the neutron.

The central [$V_c^{(\ell)}(r)$] and spin-orbit [$V_{\rm so}^{(\ell)}(r)$] radial potentials are assumed to have a Gaussian shape. In this work, four different ^{10}Be-neutron potentials (labeled as I, II, III, and IV) will be used. Their parameters for $\ell = 0$, 1, and 2 are given in Table I, and they are adjusted to reproduce the spectrum of ^{11}Be. Contributions from partial waves with $\ell > 2$ are negligibly small and not included.

TABLE I. Strengths (in MeV) and ranges (in fm) of the central and spin-orbit Gaussian potentials [$V_c^{(\ell)}(r) = S_c^{(\ell)}e^{-(r/b_c^{(\ell)})^2}$, $V_{\rm so}^{(\ell)}(r) = S_{\rm so}^{(\ell)}e^{-(r/b_{\rm so}^{(\ell)})^2}$] entering in Eq. (5) for the four interactions used in the calculations. For d waves, the radial potentials are made as the sum of two Gaussians, whose strengths and ranges are given by the corresponding two rows in the table. In potential IV, the acronym P.E.P. refers to the phase equivalent potential used in this case for s and p waves (see text).

Waves		$W_{\rm I}$	$W_{\rm II}$	$W_{\rm III}$	$W_{\rm IV}$
s	$S_c^{(\ell=0)}$	−8.40	−5.78	−8.40	P.E.P.
	$b_c^{(\ell=0)}$	3.5	4.5	3.5	P.E.P.
p	$S_c^{(\ell=1)}$	40.0	40.0	40.0	P.E.P.
	$b_c^{(\ell=1)}$	3.5	3.5	3.5	P.E.P.
	$S_{\rm so}^{(\ell=1)}$	63.52	63.52	63.52	P.E.P.
	$b_{\rm so}^{(\ell=1)}$	3.5	3.5	3.5	P.E.P.
d	$S_c^{(\ell=2)}$	−26.28	−26.28	−26.28	−26.28
		−79.6	−79.6	−33.39	−79.6
	$b_c^{(\ell=2)}$	3.5	3.5	3.5	3.5
		1.7	1.7	2.5	1.7
	$S_{\rm so}^{(\ell=2)}$	−17.52	−17.52	−17.52	−17.52
		79.6	79.6	33.39	79.6
	$b_{\rm so}^{(\ell=2)}$	3.5	3.5	3.5	3.5
		1.7	1.7	2.5	1.7

Potential I is built as follows: the range of the interactions is taken equal to 3.5 fm, which is the sum of the rms radius of the core and the radius of the neutron. For s waves, the strength is fixed to fit the experimental neutron separation energy of the $1/2^+$ state in ^{11}Be (−0.504 MeV [43]). For p waves, the two free parameters (central and spin-orbit strengths) are adjusted to reproduce the experimental neutron separation energy of the $1/2^-$ state in ^{11}Be (−0.184 MeV [43]) and to simultaneously push up the $3/2^-$ state, which is forbidden by the Pauli principle, since it is occupied by the four neutrons in the ^{10}Be core.

For the d states, it is well established that ^{11}Be has a $5/2^+$ resonance at 1.28 MeV (energy above threshold) [44–46]. The strength of the $d_{5/2}$ potential is then fixed to reproduce this resonance energy (as a pole of the S matrix), leading to a resonance width of 0.4 MeV. The most likely candidate as spin-orbit partner of the $5/2^+$ state is the known $3/2^+$-resonance at 2.90 MeV (above threshold) [46]. A Gaussian with a range of 3.5 fm fitting such $3/2^+$ energy is giving rise to a very broad resonance of roughly 1.5 MeV. Experimentally, the $5/2^+$ and $3/2^+$ states at 1.28 and 2.90 MeV are rather narrow (about 100 keV) [43]. For this reason, we have reduced the range of the $d_{3/2}$ neutron-core interaction to 1.7 fm, such that the width of the $3/2^+$ state at 2.90 MeV is also 0.4 MeV. These conditions lead to a central ($V_c^{(\ell=2)}$) and spin-orbit ($V_{\rm so}^{(\ell=2)}$) radial potentials made as a sum of two Gaussians, whose strengths and ranges are given at the bottom of Table I.

In principle the computed widths of the $5/2^+$ and $3/2^+$ resonances can be reduced by simply using smaller ranges

for the corresponding Gaussians. However, to obtain widths similar to the experimental ones, unrealistic ranges are needed, and we have then preferred to use a d-wave interaction with ranges similar to the ones for the s and p potentials. This disagreement indicates that these ^{11}Be states, besides the dominating single-neutron d waves, have admixtures of the ^{10}Be core-excited 2^+ coupled to the single-neutron s wave.

Among the different partial wave neutron-core potentials described above, the s-wave potential is probably the most crucial, since it determines the properties of the ^{11}Be ground state. The s-wave neutron-^{10}Be components are expected to give a large contribution to not only the ^{12}Be ground state but also most of the excited states. To test the dependence of the results on the details of this potential, we have in potential II increased the range of the s-wave neutron-core interaction up to 4.5 fm, modifying the strength to keep the energy of the $1/2^+$ state in ^{11}Be at the experimental value.

When constructing potential I, the range of the $d_{3/2}$ potential was reduced to obtain a width for the $3/2^+$ resonance in better agreement with the experiment. To test the importance of this choice, we have in potential III increased the range of the $d_{3/2}$ interaction to 2.5 fm. The width of the $3/2^+$ resonance (at 2.90 MeV above threshold) is then 1.1 MeV.

The ^{10}Be core has two neutrons occupying the $s_{1/2}$ shell and four neutrons in the $p_{3/2}$ shell. Therefore, the neutron-core interaction cannot bind the neutron into one of these states due to the Pauli principle. To treat this fact in a more careful way, we constructed a new neutron-core potential such that there is a deeply bound $s_{1/2}$ state (forbidden by the Pauli principle) and a second bound $s_{1/2}$ state at the experimentally known energy of -0.504 MeV. In the same way, the $p_{3/2}$ interaction has been made such that there is a bound state (also forbidden by the Pauli principle) at -6.81 MeV, which is the experimental neutron separation energy in ^{10}Be [47]. These two potentials are also taken to be Gaussians, and their strengths and ranges are given in the second and third columns of Table II. The last column gives the rms radii for a neutron sitting in the $s_{1/2}$ or $p_{3/2}$ shell in ^{10}Be. The parameters used for the Gaussian potentials have been adjusted such that, together with the proper $s_{1/2}$ and $p_{3/2}$ energies, the computed single-nucleon rms radii give rise to charge and mass rms radii for ^{10}Be in agreement with the experimental values, i.e., 2.24 and 2.30 fm, respectively [48].

We then constructed potential IV using the $s_{1/2}$ and $p_{3/2}$ interactions as the phase equivalent potentials [49] of the ones described above and given in Table II. These potentials have exactly the same phase shifts for all the energies as the original ones, but the Pauli forbidden states have been removed from the two-body spectrum. Potential IV is completed with the same $p_{1/2}$ and d-wave interactions as in potential I. In particular, the central and spin-orbit parts for p waves in potential IV are given by: $V_c^{(\ell=1)} = (2V_{p_{3/2}} + V_{p_{1/2}})/3$ and $V_{\rm so}^{(\ell=1)} = 2(V_{p_{3/2}} - V_{p_{1/2}})/3$, where $V_{p_{3/2}}$ and $V_{p_{1/2}}$ are the $p_{3/2}$ and $p_{1/2}$ potentials as described above.

TABLE II. Strengths S and ranges b used for the Gaussians describing the deep neutron-^{10}Be interaction holding Pauli forbidden states for the $s_{1/2}$ and $p_{3/2}$ waves. The last column gives the single-nucleon rms radius for each wave.

Wave	S (MeV)	b (fm)	$\langle r_n^2\rangle^{1/2}$ (fm)
$s_{1/2}$	-139.84	1.78	1.26
$p_{3/2}$	-75.5	2.3	2.72

The different ^{10}Be-neutron interactions described in this section reproduce reasonably well the known spectrum of ^{11}Be up to an excitation energy of 3.41 MeV. However, it is well established that ^{11}Be has a $3/2^-$ resonance at 2.19 MeV (above threshold) [50–52], which has been ignored in our analysis. This is because a ^{10}Be core in the 0^+ ground state cannot produce a low-lying $3/2^-$ state in ^{11}Be. The first allowed $p_{3/2}$ shell in which the halo neutron could sit is too high (even if a large ^{10}Be deformation is assumed). In fact, the $3/2^-$ state in ^{11}Be very likely corresponds to ^{9}Be (whose ground state is $3/2^-$) and two neutrons in the sd shell [44]. In other words, one of the neutrons in the fully occupied $p_{3/2}$ shell in ^{10}Be has to jump into the sd shell, which means that a description of this $3/2^-$ resonance as a ^{10}Be core plus a neutron requires the core in a negative-parity excited state. Another possibility is to have the ^{10}Be core in the excited 2^+ state and the remaining neutron in the $p_{1/2}$ shell. Therefore, when investigating how an inert core three-body model describes the ^{12}Be properties, this two-body ^{11}Be state has to be excluded. We shall later discuss the consequences of this exclusion.

IV. STRUCTURE OF ^{12}Be

To solve the angular part of the Faddeev equations [Eq. (2)], it is necessary to specify the components included in the hyperspherical harmonic expansion of the angular eigenvalues. These components should be consistent with the total angular momentum and parity of the system. For ^{12}Be, two 0^+, one 2^+, and one 1^- bound states are experimentally known. We find all of them and predict the existence of an isomeric 0^- state [53]. The components included for them in the numerical calculations are given in the first five columns in Tables III–VI. The upper part of each table refers to the components in the first Jacobi set ($\boldsymbol{x}$ between the two neutrons), while the lower part gives the components in the second and third Jacobi sets ($\boldsymbol{x}$ from the core to one of the neutrons).

The quantum numbers ℓ_x and ℓ_y are the orbital angular momenta associated to the $\boldsymbol{x}$ and $\boldsymbol{y}$ Jacobi coordinates, and they couple to the total orbital angular momentum L. The spins of the two particles connected by the $\boldsymbol{x}$ coordinate couple to s_x, which in turn couples with the spin of the third particle to the total spin S. Finally L and S couple to the total angular momentum of the three-body system. An additional quantum number to be considered is the hypermomentum $K = 2n + \ell_x + \ell_y$, whose maximum value $K_{\rm max}$ for each component is crucial to guaranteeing convergence of the eigenvalues $\lambda_n(\rho)$ up to distances at which the radial wave functions are negligible. The values of $K_{\rm max}$ used in our calculations are given by the sixth column in the tables.

TABLE III. Components included in the calculations for the 0^+ states. The upper part corresponds to the first Jacobi set ($\boldsymbol{x}$ between the two neutrons). The lower part corresponds to the second and third Jacobi sets ($\boldsymbol{x}$ from core to neutron). The sixth column gives the maximum value of the hypermomentum used for each component. The last five columns give the contribution from each component to the 0^+ wave function for potentials I, II, III, IV, and I+v_8, respectively. The two numbers for each component correspond to the 0^+_1 and 0^+_2 states, respectively.

ℓ_x	ℓ_y	L	s_x	S	$K_{\max}$	$W_{\rm I}$	$W_{\rm II}$	$W_{\rm III}$	$W_{\rm IV}$	$W_{\rm I+v_8}$
0	0	0	0	0	118	90.2	88.5	88.9	88.7	86.5
						48.3	52.5	49.3	53.9	49.1
1	1	1	1	1	80	8.2	10.3	9.4	9.4	11.9
						50.2	46.0	49.2	43.5	49.5
2	2	0	0	0	82	1.6	1.2	1.8	1.9	1.6
						1.5	1.6	1.6	2.7	1.5
0	0	0	1/2	0	118	75.5	71.5	70.1	66.6	68.9
						14.5	23.3	15.6	22.0	16.3
1	1	0	1/2	0	80	6.4	7.9	7.7	11.1	9.0
						29.8	26.5	29.2	29.8	29.5
1	1	1	1/2	1	80	7.1	9.0	8.7	7.9	10.9
						48.1	44.3	46.9	41.6	48.5
2	2	0	1/2	0	82	9.7	10.2	11.9	12.6	10.0
						4.3	3.0	4.8	3.6	3.6
2	2	1	1/2	1	82	1.2	1.4	0.7	1.6	1.3
						3.3	2.8	3.4	2.9	2.2

TABLE IV. Same as Table III, but for the 2^+ state in ^{12}Be.

ℓ_x	ℓ_y	L	s_x	S	$K_{\max}$	$W_{\rm I}$	$W_{\rm II}$	$W_{\rm III}$	$W_{\rm IV}$	$W_{\rm I+v_8}$
2	0	2	0	0	100	30.7	32.1	36.4	28.8	34.2
1	1	1	1	1	60	0.6	0.7	0.2	0.5	0.4
1	1	2	1	1	60	16.1	12.2	5.2	4.2	9.1
0	2	2	0	0	120	51.7	53.6	57.6	65.6	55.3
2	2	2	0	0	22	0.9	1.5	0.5	1.0	1.0
1	1	2	1/2	0	60	1.4	1.5	1.3	3.9	1.3
1	1	2	1/2	1	60	0.2	0.2	0.1	0.2	0.2
2	2	1	1/2	1	42	0.5	0.6	0.2	0.2	0.3
2	2	2	1/2	0	62	4.3	5.3	5.3	5.5	3.9
2	2	2	1/2	1	42	0.1	0.1	0.02	0.01	0.1
2	2	3	1/2	1	42	0.7	1.2	0.1	0.1	0.3
2	0	2	1/2	0	122	38.6	39.4	44.2	43.8	42.1
2	0	2	1/2	1	62	8.6	6.9	3.0	2.4	5.7
0	2	2	1/2	0	120	37.1	37.9	42.8	41.1	40.1
0	2	2	1/2	1	60	8.5	6.7	2.9	2.4	5.5
1	1	1	1/2	1	60	0.1	0.1	0.1	0.3	0.1

TABLE V. Same as Table III, but for the 0^- state in ^{12}Be.

ℓ_x	ℓ_y	L	s_x	S	$K_{\max}$	$W_{\rm I}$	$W_{\rm II}$	$W_{\rm III}$	$W_{\rm IV}$	$W_{\rm I+v_8}$
1	0	1	1	1	119	97.6	95.3	97.5	96.6	98.0
1	2	1	1	1	41	2.4	4.7	2.5	3.3	2.0
0	1	1	1/2	1	99	54.2	53.8	54.3	54.2	54.3
1	0	1	1/2	1	99	45.4	45.8	45.4	45.3	45.4
2	1	1	1/2	1	41	0.1	0.1	0.1	0.2	0.1
1	2	1	1/2	1	41	0.3	0.3	0.2	0.2	0.2

TABLE VI. Same as Table III, but for the 1^- state in ^{12}Be.

ℓ_x	ℓ_y	L	s_x	S	$K_{\max}$	$W_{\rm I}$	$W_{\rm II}$	$W_{\rm III}$	$W_{\rm IV}$	$W_{\rm I+v_8}$
1	0	1	1	1	119	60.2	58.5	59.8	46.2	60.3
0	1	1	0	0	99	36.8	36.2	36.9	50.4	36.7
2	1	1	0	0	61	0.7	1.4	0.7	0.6	0.7
1	2	1	1	1	81	2.2	3.9	2.5	2.6	2.2
1	2	2	1	1	61	0.1	0.04	0.1	0.2	0.1
1	0	1	1/2	0	99	19.8	19.7	19.7	25.4	19.6
1	0	1	1/2	1	119	28.6	28.9	28.6	22.8	28.6
0	1	1	1/2	0	99	16.6	16.7	16.6	21.5	16.4
0	1	1	1/2	1	119	33.9	33.5	33.8	26.6	33.9
1	2	1	1/2	0	41	0.3	0.3	0.4	1.4	0.4
1	2	1	1/2	1	41	0.3	0.3	0.3	0.3	0.3
1	2	2	1/2	1	41	0.04	0.03	0.1	0.1	0.1
2	1	1	1/2	0	41	0.4	0.4	0.5	1.7	0.5
2	1	1	1/2	1	41	0.05	0.05	0.04	0.1	0.1
2	1	2	1/2	1	41	0.05	0.04	0.1	0.1	0.1

A. Effective potentials

The angular eigenvalues obtained from Eq. (2) enter into the coupled set of radial equations (3) as a part of the effective potentials $V^{(n)}_{\rm eff}(\rho) = \frac{1}{\rho^2}\left(\lambda_n(\rho) + \frac{15}{4}\right)$. In Fig. 1, we show the three most contributing effective potentials for the 0^+, 2^+, 1^-, and 0^- states in ^{12}Be. The results using potential I for the neutron-core interaction and the Gaussian neutron-neutron potential are shown by the solid curves. When potential IV is used (dashed curves) these potentials are noticeably different in amplitude from the ones with potential I, but, in general, have similar shape. The following effective adiabatic potentials behave very similarly in both cases. When the neutron-core potentials II and III are used, only minor differences in the adiabatic potentials are found compared to the ones obtained

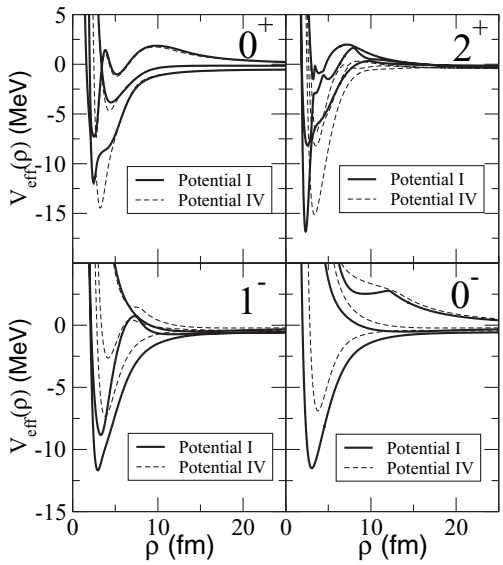

FIG. 1. Three lowest adiabatic effective potentials for the 0^+, 2^+, and 1^- states in ^{12}Be. Results using the neutron-core potentials I and IV are shown.

TABLE VII. Spectrum of ^{12}Be for the different neutron-core interactions (see Table I). The numerical results have been obtained without inclusion of a three-body potential in Eq. (3). In the sixth column, potential I has been used together with the v_8-Argonne nucleon-nucleon interaction. The energies are given in MeV.

	$W_{\rm I}$	$W_{\rm II}$	$W_{\rm III}$	$W_{\rm IV}$	$W_{\rm I+v_8}$	Exper.
0^+_1	−3.60	−3.22	−3.64	−3.77	−3.53	−3.67[a]
2^+	−0.54	−0.36	−0.66	−0.96	−0.58	-1.56 ± 0.01[b]
0^+_2	−0.62	−0.64	−0.64	−0.61	−0.74	-1.43 ± 0.02[c]
1^-	−0.97	−0.97	−0.97	−1.23	−1.12	-0.99 ± 0.03[d]
0^-	−0.96	−0.89	−0.96	−0.93	−1.17	—

[a]From Ref. [43].
[b]From Ref. [30].
[c]From Ref. [34].
[d]From Ref. [32].

with potential I. All the neutron-core interactions give rise to indistinguishable effective potentials at large distances. For the 0^+ and 0^- cases, the deepest and second deepest effective potentials go asymptotically to −0.504 and −0.184 MeV, respectively, which are the two-body binding energies of the bound states in ^{11}Be. For 1^- and 2^+, the two deepest effective potentials go asymptotically to −0.504 MeV and the third deepest to −0.184 MeV.

B. Three-body energy spectrum

After solving the coupled set of radial equations [Eq. (3)], we obtain a series of ^{12}Be bound states whose two-neutron separation energies are given in Table VII. Columns 2 to 5 show the results obtained with the ^{10}Be-neutron interactions given in Table I. The Gaussian neutron-neutron potential is used. To test the role played by the short-distance details of the nucleon-nucleon interaction, we give in the sixth column the spectrum obtained when potential I is combined with the Argonne v_8 neutron-neutron interaction. The last column gives the available experimental values. These results correspond to calculations without fine tuning the effective three-body potentials with a three-body force [$V_{\rm 3b}(\rho) = 0$ in Eq. (3)].

The bound states found can be understood assuming a simple extreme single-particle model: the ground 0^+ state should correspond to a configuration in which the two neutrons occupy the two $s_{1/2}$ single-neutron states. The 1^- and the 0^- can be understood as one neutron in the $s_{1/2}$ wave and the other one in a $p_{1/2}$ state. The 2^+ state appears with one neutron in the $s_{1/2}$ wave and the second in the $d_{5/2}$ state, and finally, the second 0^+ state corresponds to both neutrons in $p_{1/2}$ waves.

For the 0^+_1 ground state, all the computed energies are similar, except for potential II, which is clearly less bound than the rest. In potential II, the s-wave neutron-core potential employed a larger range (see Table I). Since the structure of the 0^+_1 state is expected to be dominated by the s-wave components, an increase of the range for this wave increases the spatial extension of the system and subsequently decreases the binding energy. In potential IV, the s-wave interaction has been constructed in a completely independent way compared to potentials I, II, and III. The fact that in this case the binding energy of the ground state is similar (actually slightly more bound) than for potentials I and III indicates that a range of 3.5 fm for the s-wave interaction could be more appropriate.

The p-wave potential is identical for cases I, II, and III. Potential IV also uses the same $p_{1/2}$ interaction but different $p_{3/2}$, which, however, is expected to play a minor role because of the Pauli principle. This explains why the energy of the 0^+_2 state is very much the same for all neutron-core potentials, since this state should be dominated by a pp configuration.

For the 1^- (or 0^-) and 2^+ states a neutron in the $s_{1/2}$ wave is combined with the second neutron in either the $p_{1/2}$ or $d_{5/2}$ state, respectively. These states are less bound than the ground state. The effect of this is more important than the confining effects of the p and d centrifugal barriers, and consequently the 1^- (or 0^-) and 2^+ states are more extended than the ground state. Therefore the effect of the larger range in potential II for the s-wave interaction should be smaller. Actually, the 1^- energy is the same for all three potentials.

In potential IV, the d-wave interaction is the same as in potential I. Also the s-wave and p-wave potentials, although obtained in a completely different way, produce similar 0^+ states. However, the 1^- state, and especially the 2^+ state, are more bound than with potential I. This indicates that the sp and sd interferences for these states differ between potentials IV and I. When the Gaussian neutron-neutron interaction is substituted by the v_8-Argonne potential (sixth column in Table VII) similar results are found. Only a little more binding is found for the 1^-, 0^-, and 0^+_2 states.

In summary, the energies obtained with the different potentials are quite stable, and the small differences found for some of the cases are insignificant, especially when taking into account the level of accuracy of the calculations at this stage. In fact, when compared with the experimental energies (last column of Table VII), we see that in some cases the computed energy really disagrees with the experimental value, and even the ordering of the levels does not agree with the experiment. However, the ordering of the computed levels agrees with the extreme single-particle model. The ground state should be the one having the two neutrons in the deepest single-neutron level (the 0^+_1 state having both neutrons in the $s_{1/2}$ wave). The first excited state should appear when one neutron jumps into the next single-neutron level (the 1^- or the 0^- state having one neutron in the $s_{1/2}$ wave and the other one in the $p_{1/2}$ wave). Finally, the states corresponding to the $p_{1/2}$-$p_{1/2}$ and the $s_{1/2}$-$d_{5/2}$ configurations (0^+_2 and 2^+ states) should in principle be less bound than the 1^- and the 0^- states.

C. Angular momentum decomposition

It is important to keep in mind that part of the contributions arising from core deformation have been effectively taken into account by fitting the parameters in the two-body potentials to the ^{11}Be data. In this sense, the different states found in the ^{12}Be spectrum are sensitive to such deformation. However, with such two-body interactions and the core treated as an inert particle, the additional contributions arising from the 2^+ excited state in ^{10}Be are expected to play a minor role

for both the 0^+_1 and 1^- states. For the ground state, this is because two neutrons in the $s_{1/2}$-shell and a core in a 2^+ state cannot produce total angular momentum zero. For the 1^- state, it is because although a core in a 2^+ state and the two neutrons in the $s_{1/2}$-$p_{1/2}$ configuration can produce a total angular momentum 1, this structure is obviously less favorable energetically than with the core in the ground state. However, for the 2^+ state, it could be energetically efficient to excite the core into the 2^+ state and get some extra binding by placing the two neutrons in a $s_{1/2}$-$s_{1/2}$ configuration. The same could happen for the second 0^+ state, in which it could be favorable to excite the core into the 2^+ state and place the neutrons in the $s_{1/2}$-$d_{5/2}$ configuration. Therefore, the disagreement between the computed and experimental binding energies of the 2^+ and 0^+_2 states could be a signal of the importance of core excitations for these two particular states.

In any case, the deviations between computed and experimental energies are quite common when three-body calculations are performed with bare two-body interactions. All those effects going beyond the two-body correlations have obviously not been considered in the calculations. Among them are those arising from contributions of core deformation and/or core excitation. The usual cure for this problem is to include an effective three-body potential $V_{3b}(\rho)$ that simulates the neglected effects. Since these effects should appear when all three particles are close to each other, the three-body potential should be of short-range character.

In our calculations, we have used a Gaussian three-body force, whose range has been taken equal to 4.25 fm, which is the hyperradius corresponding to a ^{10}Be core and two neutrons touching each other. The strength of the Gaussian is adjusted to match the experimental energies given in the last column of Table VII.

Since the 0^- state is unknown experimentally, we cannot use its energy to adjust the strength of the three-body force. However, in this case, we expect the three-body correction to be unimportant because of the similarity of the 0^- state to the composition of the 1^- state where the experimental energy is reproduced without any three-body force. This indicates that the computed 0^- energy also is close to the correct value.

Including the three-body potentials, we have the four potentials specified in Table I, and in addition, we have potential I combined with the v_8-Argonne neutron-neutron potential. We then arrive at the contributions of the different partial wave components given in the last five columns of Tables III–VI for the 0^+, 2^+, 0^-, and 1^- states. The dominating components are in all the cases as expected from the extreme single-particle picture. When the three-body wave functions are written in the second or third Jacobi set ($\boldsymbol{x}$ from core to neutron, lower part of the tables) the dominating components are the $\ell_x = \ell_y = 0$ ($\sim$70%) for the 0^+_1 ground state, the $\ell_x = \ell_y = 1$ ($\sim$ 75%) for the 0^+_2 state, the $\{\ell_x = 0, \ell_y = 2\}$ and $\{\ell_x = 2, \ell_y = 0\}$ components ($\sim$ 90% in total) for the 2^+ state, and the $\{\ell_x = 0,\ \ell_y = 1\}$ and $\{\ell_x = 1, \ell_y = 0\}$ components ($\sim$ 98% and $\sim$ 99% in total) for the 1^- and 0^- states. Although the precise numbers can change a little from one potential to another, the differences are not significant. The residual contributions are more relevant for the 0^+ states. The ground state has a p-wave contribution of about 13–19%, and a d-wave contribution of about 10–13%. The second 0^+ state has an s-wave contribution from 15% to 23%, and a d-wave contribution from 6% to 8%.

In Ref. [12], the configuration with the two outer neutrons in the p shell for the 0^+ ground state amounts to 32% of the wave function, which is clearly larger than the 13–19% obtained in this work. In Ref. [2], this value is given to range between 20% and 40%. Correspondingly, the contribution from configurations with the two neutrons in the sd shell is larger in our calculation than in Refs. [2,12]. In these two references, the individual contributions from s and d waves are not given. In general, for both ^{11}Li and ^{12}Be, the s-wave components are larger in cluster models than in shell model calculations. One reason for ^{12}Be is that the d waves are underestimated in the cluster model because of the neglect of the core-excited 2^+ state. Another reason could be that large spatial extension is harder to describe in shell models than in cluster models. Since s waves for a given energy extend to larger distances than d waves, the shell model tends to underestimate the s-wave components. As we will show later, the contributions obtained in the present work are consistent with the measured invariant mass spectrum given in Ref. [13].

D. Wave functions

The rms radii for the computed bound states are given in Table VIII. The results are essentially independent of the core-neutron potential used. The only available experimental value is the one corresponding to the 0^+_1 ground state [48], for which a good agreement between theory and experiment is found.

The geometry of the different states is reflected in the results given in Table IX, where we give the rms distances between the two neutrons ($\langle r^2_{nn}\rangle^{1/2}$), and between the core and one of the neutrons ($\langle r^2_{cn}\rangle^{1/2}$) for the different cases. The ground state corresponds mainly to the three particles placed in the vertices of an equilateral triangle. For the excited states, the smaller binding obviously implies a larger distance between particles. But, as seen in Table IX, the distance between the neutrons grows clearly faster than the one between the neutron and the core. In fact, for the less bound excited states (the 1^- and 0^- states) the distance between the two neutrons is roughly a

TABLE VIII. Root mean square radii (in fm) for the different bound states in ^{12}Be with the four neutron-core interactions. A Gaussian three-body forced is included to fit the experimental binding energies. The range of the three-body force is 4.25 fm. Sixth column is as potential I $+v_8$ Argonne nucleon-nucleon interaction.

	$W_{\rm I}$	$W_{\rm II}$	$W_{\rm III}$	$W_{\rm IV}$	$W_{\rm I+v_8}$	Exper.
0^+_1	2.60	2.63	2.60	2.61	2.60	2.59 ± 0.06[a]
2^+	2.72	2.74	2.68	2.70	2.67	—
0^+_2	2.88	2.91	2.87	2.90	2.87	—
1^-	3.23	3.24	3.23	3.19	3.16	—
0^-	3.18	3.35	3.18	3.18	3.00	—

[a]From Ref. [48].

TABLE IX. For the different computed states in ^{12}Be, and the different neutron-core potentials, rms distances (in fm) $\langle r_{nn}\rangle^{1/2}$ and $\langle r_{cn}\rangle^{1/2}$, where n and c denote an external neutron and the core, respectively. A Gaussian three-body force is included to fit the experimental binding energies.

		$W_{\rm I}$	$W_{\rm II}$	$W_{\rm III}$	$W_{\rm IV}$	$W_{\rm I+v_8}$
0_1^+	$\langle r_{nn}^2\rangle^{1/2}$	4.5	4.6	4.4	4.3	4.4
	$\langle r_{cn}^2\rangle^{1/2}$	4.0	4.1	4.0	4.1	4.0
2^+	$\langle r_{nn}^2\rangle^{1/2}$	5.7	5.8	5.4	5.2	5.4
	$\langle r_{cn}^2\rangle^{1/2}$	4.4	4.5	4.3	4.4	4.3
0_2^+	$\langle r_{nn}^2\rangle^{1/2}$	7.3	7.8	7.3	7.7	7.3
	$\langle r_{cn}^2\rangle^{1/2}$	5.0	5.1	5.0	5.1	5.0
1^-	$\langle r_{nn}^2\rangle^{1/2}$	8.8	9.2	8.7	8.1	8.3
	$\langle r_{cn}^2\rangle^{1/2}$	6.4	6.7	6.4	6.1	6.0
0^-	$\langle r_{nn}^2\rangle^{1/2}$	9.2	9.9	9.2	9.2	8.4
	$\langle r_{cn}^2\rangle^{1/2}$	6.0	6.4	5.9	6.0	5.4

factor of 2 larger than the corresponding distance in the ground state, while the neutron-core distance increases by a factor of 1.5.

The spatial distribution of the three constituents can be better seen in Figures 2–6, where we show the probability distribution for the $0_1^+, 0_2^+, 2^+, 1^-$, and 0^- states in ^{12}Be. The probability distribution is defined as the square of the three-body wave functions multiplied by the phase-space factors and integrated over the directions of the two Jacobi coordinates. In particular, in the figures, we have chosen the first Jacobi set such that the distributions are plotted as functions of the distance between the two neutrons (r_{nn}) and the distance between the core and the center of mass of the two neutrons ($r_{c,nn}$), respectively. The 0_1^+ and the 2^+ states have the largest probabilities when the two neutrons are separated from each other almost the same distance as from the core (about 2.2 and 2.6 fm, respectively). On the other hand, $0_2^+, 0^-$, and 1^- states have the largest probabilities when the two neutrons are well separated from each other (about 5.5 fm) while they are closer to the core (about 3.5 fm). The 2^+ state has also a secondary probability maximum with this last geometry.

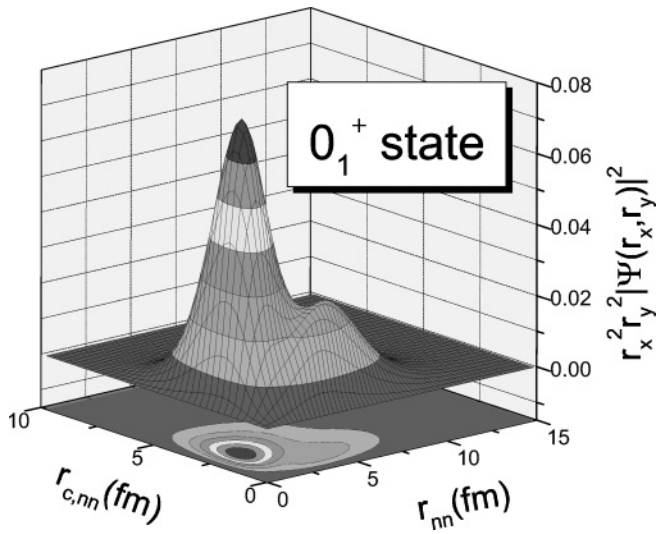

FIG. 2. Contour diagram for the probability distribution of 0_1^+ state in ^{12}Be. The square of the three-body wave function is integrated over the directions of the two Jacobi coordinates.

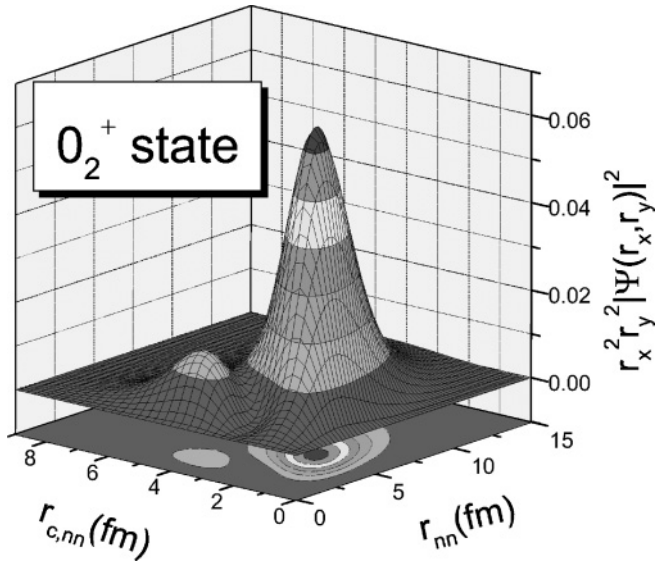

FIG. 3. Same as Fig. 2, but for the 0_2^+ state in ^{12}Be.

V. TRANSITION STRENGTHS

The bound states can only decay electromagnetically. The corresponding observable transition probabilities are critically dependent on the structures. Thus they provide experimental tests, and we therefore compute the lifetimes for future comparison. The selection rules determine the dominating transitions which can be of both electric and magnetic origin.

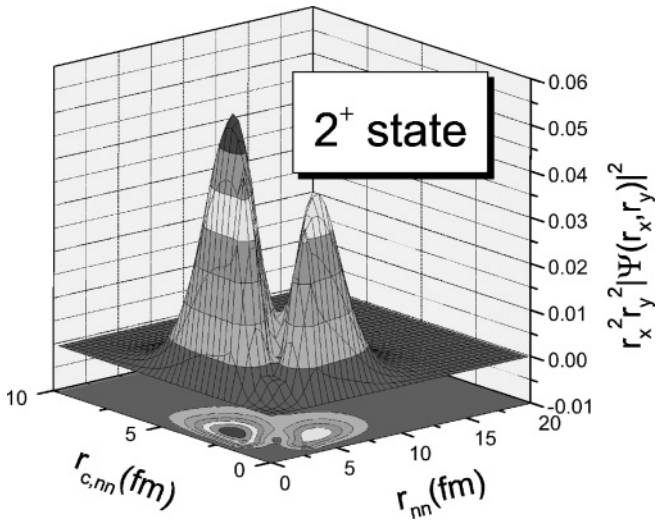

FIG. 4. Same as Fig. 2, but for the 2^+ state in ^{12}Be.

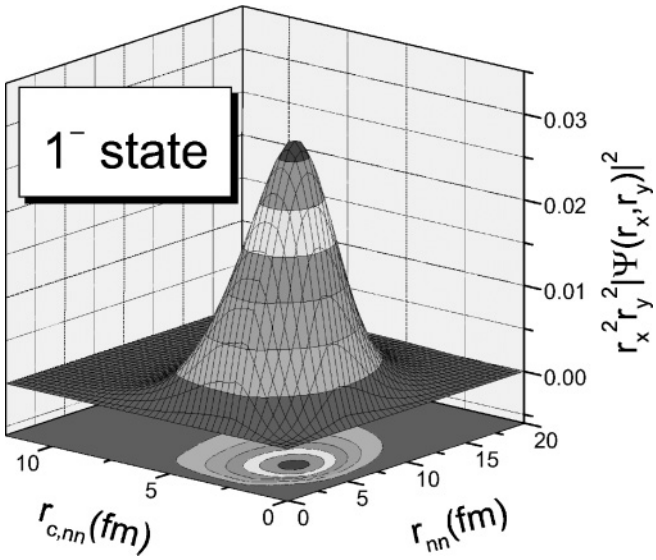

FIG. 5. Same as Fig. 2, but for the 1^- state in ^{12}Be.

A. Electric transitions

The electric multiple operators are defined as

$$\mathcal{M}_\mu(E\lambda) = e \sum_{i=1}^{A} Z_i r_i^\lambda Y_{\lambda,\mu}(\hat{r}_i), \tag{6}$$

where A is the number of constituents in the system, eZ_i is the charge of constituent, and $\boldsymbol{r}_i$ is its coordinate relative to the A-body center of mass.

The electric multipole strength functions are defined as

$$\begin{aligned}\mathcal{B}(E\lambda, I_i \to I_f) &= \sum_{\mu M_f} |\langle I_f M_f | \mathcal{M}_\mu(E\lambda) | I_i M_i \rangle|^2 \\ &= \frac{1}{2I_i + 1} |\langle I_f || \mathcal{M}(E\lambda) || I_i \rangle|^2. \end{aligned} \tag{7}$$

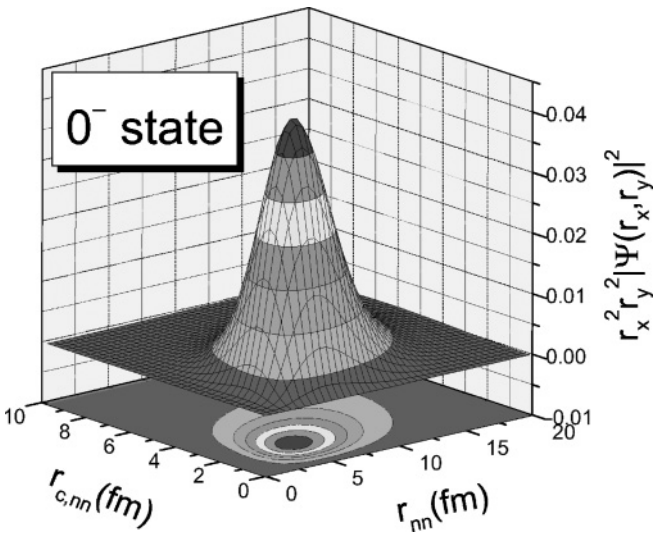

FIG. 6. Same as Fig. 2, but for the 0^- state in ^{12}Be.

Also, following Ref. [40], we consider the monopole transition operator

$$\mathcal{M}_0(E0) = e \sum_{i=1}^{A} Z_i r_i^2. \tag{8}$$

In our three-body model, where $A-2$ constituents are assumed to form a well-defined core, the operators (6) and (8) contain one term directly associated with the three-body system having the form

$$\mathcal{M}_\mu(E\lambda) = e \sum_{i=1}^{3} Z_i r_i^\lambda Y_{\lambda,\mu}(\hat{r}_i), \tag{9}$$

$$\mathcal{M}_0(E0) = e \sum_{i=1}^{3} Z_i r_i^2, \tag{10}$$

where i labels the three constituents. In addition to Eqs. (9) and (10), there is a contribution from the intrinsic core multipole operators. In particular, for the electric dipole and quadrupole operators, the precise expressions are given by Eqs. (A3) and (A4). For the quadrupole case, Eq. (A4), an additional contribution arises from the coupling between the electric dipole operator of the core and its motion around the three-body center of mass.

When an inert core has spin zero, as in the present ^{12}Be model, the contributions from the intrinsic core multipole operators $\mathcal{M}_\mu(E\lambda, \text{core})$ are zero. These terms contribute only when core excitations are included. For ^{12}Be, the first excited state of the ^{10}Be core is a 2^+ state at about 3.4 MeV. Its effect on the $\mathcal{B}(E1)$ strength must be small, since the $\mathcal{M}_\mu(E1, \text{core})$ operator does not couple the 0^+ and 2^+ core states. Therefore the $\mathcal{B}(E1)$ strength is expected to be less dependent on the contribution of the 2^+ excited state in the core than the $\mathcal{B}(E2)$ strength, where the $\mathcal{M}_\mu(E2, \text{core})$ operator does couple the 0^+ and 2^+ states in the core.

Also, the $\mathcal{M}_0(E0, \text{core})$ operator is not coupling the 0^+ and 2^+ states of the core. However, the expectation value of this operator between the 0^+ ground state of the core is not zero (it is actually related to the rms radius of the core). Nevertheless, for an inert core with spin zero, the total nuclear wave function factorizes into the three-body cluster wave function and the core wave function. In this way, the expectation value of $\mathcal{M}_0(E0, \text{core})$ between wave functions corresponding to different states is automatically zero because of the orthogonality of the three-body cluster wave functions.

For ^{11}Be (^{10}Be+n), the experimental value of the $\mathcal{B}(E1, \frac{1}{2}^- \to \frac{1}{2}^+)$ transition strength is $0.115 \pm 0.010\, e^2$ fm^2 [54]. Direct application of Eq. (9) assuming zero charge for the neutrons fails to reproduce this value. However, it is well known that to take into account the distortion or polarization of the core, one has to include an effective charge for the neutrons [55,56]. Because of the square in Eq. (7), two different neutron effective charges are found to fit the experimental value for $\mathcal{B}(E1, \frac{1}{2}^- \to \frac{1}{2}^+)$: $Z_n = 0.28$ and $Z_n = 0.52$. These two charges give rise to slightly different mean square charge radii for the ground state in ^{11}Be of about 2.7 and 3.0 fm, respectively. The ^{10}Be-neutron potential has only a marginal effect, and only 2.7 fm is consistent with the experimental value

TABLE X. $\mathcal{B}(E1)$ (in e^2 fm^2), $\mathcal{B}(E2)$ (in e^2 fm^4) transition strengths between the computed states in ^{12}Be given in Table VII and $\mathcal{M}(E0)$ (in e fm^2) between the two 0^+ states. An effective three-body force has been used to fit the experimental binding energies.

	$W_{\rm I}$	$W_{\rm II}$	$W_{\rm III}$	$W_{\rm IV}$	$W_{\rm I+v_8}$	Exper.
$\mathcal{B}(E1, 0_1^+ \to 1^-)$	0.046	0.052	0.048	0.064	0.051	0.051 ± 0.013[a]
$\mathcal{B}(E1, 0_2^+ \to 1^-)$	0.016	0.006	0.016	0.010	0.015	–
$\mathcal{B}(E1, 2^+ \to 1^-)$	0.0054	0.0074	0.0079	0.018	0.0081	–
$\mathcal{B}(E2, 2^+ \to 0_1^+)$	3.14	3.50	3.52	3.93	3.04	$5.5 - 8.2$[b]
$\mathcal{B}(E2, 2^+ \to 0_2^+)$	0.024	0.32	0.044	0.12	0.047	1.40 ± 0.12[c]
$\mathcal{M}(E0, 0_2^+ \to 0_1^+)$	1.89	0.60	1.77	1.13	1.99	0.87 ± 0.03[c]

[a]From Ref. [32].
[b]Estimation from experimental data in Ref. [31].
[c]From Ref. [40].

of 2.63 ± 0.05 fm [48]. Therefore, a neutron effective charge of $Z_n = 0.28$ has been used in the following calculations.

In Table X, we give the computed $\mathcal{B}(E\lambda)$ values for transitions between the states in Table VII and the monopole transition matrix element $\mathcal{M}(E0) \equiv |\langle 0_2^+ | \mathcal{M}_0(E0) | 0_1^+ \rangle|$. An effective three-body force has been included to fit the experimental binding energies for the different ^{12}Be states. The results are quite stable for the different neutron-core potentials used. The only exceptions are the transitions in which the 0_2^+ state is involved. This state is the one showing the most important dependence on the potential used. In particular, potentials II and IV produce an s-wave content (lower part of Table III) about 50% larger than that of potentials I and III. As seen in the table, the results are sensible to this difference, since the values found for $\mathcal{B}(E2, 2^+ \to 0_2^+)$, $\mathcal{B}(E1, 0_2^+ \to 1^-)$, and $\mathcal{M}(E0)$ with potentials II and IV clearly differ from the ones with I and III.

For the $\mathcal{B}(E1)$ transitions, the experimental value of 0.051 ± 0.013 e^2 fm^2 corresponding to the $0_1^+ \to 1^-$ transition [32], agrees well with the results given in the first row of Table X. The agreement is equally good for all the neutron-core potentials used. Only for potential IV the computed value is a bit higher than for the other cases, but the computed result is still lying within the experimental error. Therefore the three-body model used reproduces well the experimental value, although it is worth emphasizing that the effective neutron charge also is introduced to simulate neglected effects of core deformation and polarization. The small effect from the three-body potential can be attributed to the choice of minimal structure, which means no dependence on angular momentum quantum numbers. The only essential effect is an adjustment of the three-body energy, which in turn may have an effect on the spatial extension, but leaving all structures unchanged. For the other two $E1$ transitions, experimental data are not available.

Using the same effective neutron charge, we get the $\mathcal{B}(E2)$ values in the central part of Table X. Assuming that the 2^+ state in ^{12}Be is a rotational state built on the ground state, an experimental value of 2.00 ± 0.23 is given in Ref. [31] for the deformation length δ in ^{12}Be. This assumption means that the $\mathcal{B}(E2, 2^+ \to 0_1^+)$ value is given by $\frac{1}{5}(\frac{3}{4\pi} Ze\delta)^2 R^2$, which equals 5.5 ± 1.3 or $8.2 \pm 1.9 e^2$ fm^4 for $R \approx 1.2A^{1/3}$ fm or $R = \sqrt{5/3}\langle r^2 \rangle^{1/2}$, respectively. Here $\langle r^2 \rangle^{1/2}$ is the experimental charge rms radius of ^{12}Be. Both values are higher than obtained numerically (first line in the central part of the table).

Also, the recently measured value of $1.40 \pm 0.12 e^2$ fm^4 [40] for $\mathcal{B}(E2, 2^+ \to 0_2^+)$ is much larger than all the computed results in the table, which varies about one order of magnitude with the different neutron-core potentials. Furthermore, we see that the computed $\mathcal{B}(E2, 2^+ \to 0_1^+)$ is much larger than $\mathcal{B}(E2, 2^+ \to 0_2^+)$. This arises from the fact that the 2^+ state is dominated by the sd interferences in the second and third Jacobi sets (lower part of Table IV), while the 0_2^+ state is dominated by a pp configuration (lower part of Table III). When the core is infinitely heavy, these dominating configurations must give a vanishing contribution from Eq. (9) to the $\mathcal{B}(E2, 2^+ \to 0_2^+)$ value. Thus, the values in Table X have to be small and very sensitive to the nondominating components in the two states.

Small variations in the contribution of some of these smaller components can produce large relative changes in the computed transition strength. In particular, for the 0_2^+ state, the $\ell_x = 1$ components clearly dominate, but a substantial probability appears in the $\{\ell_x = 0, S = 0\}$ component, which coincides with a large probability for the $\{\ell_x = 0, S = 0\}$ component in the 2^+ state, see the lower part of Table IV. For potentials II and IV, this s-wave component in the 0_2^+ state (Table III) is significantly larger than for the other three potentials. This implies a larger overlap, and therefore a larger $\mathcal{B}(E2)$ transition strength.

At this point, it is important to emphasize that the computed results are obtained for an inert core. For $E2$ transitions, a non-negligible contribution from the 2^+ excited state in the ^{10}Be core is expected. The second term in the electric quadrupole operator (A4), together with the existence of the core excited 2^+ state, gives rise to another nonvanishing contribution. In fact, for ^{10}Be, the experimental $\mathcal{B}(E2, 2^+ \to 0^+)$ transition strength is known to be $10.4 e^2$ fm^4 [57]. Thus the computed three-body $\mathcal{B}(E2)$ values should be supplemented by the contribution of $10.4 e^2$ fm^4 multiplied by the weight factor corresponding to the admixtures of the 2^+ core excitation in

the ^{12}Be states. In fact, this contribution should provide most of the strength for the $2^+ \to 0_2^+$ transition. In contrast, the contribution from the last term in the quadrupole transition operator (A4) is expected to be small, since $\mathcal{M}_\mu(E1, \text{core})$ cannot couple 0^+ and 2^+ states.

In Ref. [40], an experimental value of $0.87 \pm 0.03e$ fm^2 is given for the monopole transition matrix element between the two 0^+ states. This observable gives information about the relative structures of these two states. The computed results are given in the last row of Table X, and they are clearly higher (except for potential II) than the experimental value, but similar to the value of $1.7e$ fm^2 obtained in Ref. [58]. However, as seen in the table, the computed results are very sensitive to the contribution of the relative neutron-^{10}Be s wave. An increase from about 15% to 23% reduces the computed $\mathcal{M}(E0)$ by a factor of 3 (going in fact through the experimental value). This s-wave contribution could easily change significantly when core excitations are included in the 0_2^+ wave function, for which, as mentioned at the beginning of Sec. IV C, such excitations could play a relevant role.

B. Magnetic transitions

For the unobserved predicted 0^- state, the dominating multipolarities for its possible decays are of magnetic character. Only $M1$ and $M2$ transitions to the 1^- or the 2^+ states are possible.

The magnetic multiple operator is defined as

$$\mathcal{M}_\mu(M\lambda) = \frac{e\hbar}{2Mc}\sqrt{\lambda(2\lambda+1)}\sum_i r_i^{\lambda-1}\left[\left(g_s^{(i)} - \frac{2g_\ell^{(i)}}{\lambda+1}\right)(Y_{\lambda-1}s) + \frac{2g_\ell^{(i)}}{\lambda+1}(Y_{\lambda-1}j)\right]_{(\lambda-1,1)\lambda\mu}, \tag{11}$$

where the constants g_s and g_ℓ depend on the constituent particles i. The magnetic multipole strength functions are defined as for the electric case [see Eq. (7)].

In particular, the $\mathcal{M}1$ and $\mathcal{M}2$ operators involved in the magnetic dipole and quadrupole decay of the 0^- state into the 1^- and 2^+ states are

$$\mathcal{M}_\mu(M1) = \frac{e\hbar}{2Mc}\sqrt{\frac{3}{4\pi}}\sum_i \left(g_s^{(i)}\vec{s}_i + g_\ell^{(i)}\vec{\ell}_i\right)_\mu, \tag{12}$$

$$\mathcal{M}_\mu(M2) = \frac{e\hbar}{Mc}\frac{5}{\sqrt{2}}\sum_i\sum_{\nu,q}\begin{pmatrix}1 & 1 & 2\\ \nu & q & -\mu\end{pmatrix}Y_{1,\nu}(\Omega_i) \times\left(g_s^{(i)}\vec{s}_i + \frac{2g_\ell^{(i)}}{3}\vec{\ell}_i\right)_q, \tag{13}$$

where q labels the spherical component of an operator.

We can identify a source of uncertainties in the transition strength estimates, which comes from the effective values of the g factor in these expressions.

The core has angular momentum zero and therefore a vanishing effective spin $g_s^{(c)}$ factor and $g_\ell^{(c)} = 4$. We also use the free value of $g_s^{(n)} = -3.82$, and we use again an effective neutron charge $g_\ell^{(n)} = 0.28$. The transition operators are then defined, and we can compute the $\mathcal{B}(M1, 0^- \to 1^-)$ and $\mathcal{B}(M2, 0^- \to 2^+)$ transition strengths. The results are given in Table XI, where we observe that the computed values are rather independent of the particular neutron-core potential used. Only for potential IV, the results deviate by up to a factor of 2 from the other estimates. This reflects the fact that potential IV is producing a different distribution of the weights between the components in the 1^- and 2^+ states (see Tables VI and IV).

TABLE XI. $\mathcal{B}(M1)$ (in e^2 fm^2) and $\mathcal{B}(M2)$ (in e^2 fm^4) transition strengths between the computed states in ^{12}Be given in Table VII. An effective three-body force has been used to fit the experimental binding energies.

	W_{I}	W_{II}	W_{III}	W_{IV}	$W_{\text{I}+v_8}$
$\mathcal{B}(M1, 0^- \to 1^-)$	0.060	0.061	0.059	0.049	0.061
$\mathcal{B}(M2, 0^- \to 2^+)$	0.94	0.78	0.78	0.43	0.85

As mentioned above, the effective values of the g factors are rather uncertain, and spin polarization could reduce g_s by a factor of 2, change $g_\ell^{(c)}$ by perhaps 10%, and vary $g_\ell^{(n)}$ from the assumed effective value (see also the discussion of the empirical evidence in Ref. [59]). As discussed in Ref. [53], the computed magnetic strength has a very limited dependence on the precise values used for the orbital gyromagnetic factors g_ℓ, and they are mainly only sensitive to $g_s^{(n)}$. In particular, use of $g_s^{(n)} = -2.0$ reduces the computed magnetic strengths by a factor of about 3.

In summary, the decay possibilities for the 0^- state are limited to magnetic transitions. Even with fairly reliable estimates for the transition probabilities, it is not easy to give an accurate prediction for the lifetime of this state. If 0^- is below the 1^- state, only decay into 2^+ is possible and the resulting lifetime can be estimated to be of the order 10^{-8} s. However, if 0^- can decay into the 1^- state, the possibly very small energy difference causes a large uncertainty which could reduce the lifetime to about 10^{-11} s or perhaps even somewhat smaller. In any case, these estimates justify the classification of this new 0^- state as an isomer in ^{12}Be.

VI. INVARIANT MASS SPECTRUM

One tool for studying the structure of three-body halo nuclei is to use information obtained from breakup reactions. The relatively fast removal of one of the constituents leaves the remaining two essentially undisturbed, and measurements of their momenta then provide fairly direct information about the initial state. We use this technique to investigate the two-body substructures of ^{12}Be. The experimental relative ^{10}Be-neutron energy spectrum (or invariant mass spectrum) after ^{12}Be breakup on a carbon target at a beam energy of 39.3 MeV/nucleon is shown in Ref. [13]. Both fragments, ^{10}Be and neutron, are simultaneously detected, and their relative decay energy is reconstructed from the measured momenta. The final ^{10}Be-neutron states are then restricted to unbound states in ^{11}Be.

This spectrum can easily be computed by use of the sudden approximation. We assume that the target transfers a (relatively

large) momentum to one of the particles (one of the neutrons) in the projectile which then is instantaneously removed. The remaining two particles, the ^{10}Be core and the second neutron, are just spectators in the reaction, meaning that they continue their motion undisturbed without further interaction with the removed particle. They do, however, continue to interact with each other.

Under this assumption, the differential cross section of the process takes the form

$$\frac{d^6\sigma}{d\boldsymbol{k}_x\, d\boldsymbol{k}_y} \propto \sum_M \sum_{s_x\sigma_x\sigma_y} \left|\langle e^{i\boldsymbol{k}_y\cdot\boldsymbol{y}}\chi_{s_y}^{\sigma_y} w_{s_x}^{\sigma_x}(\boldsymbol{k}_x,\boldsymbol{x})|\Psi^{JM}(\boldsymbol{x},\boldsymbol{y})\rangle\right|^2, \tag{14}$$

where Ψ^{JM} is the three-body wave function with total angular momentum J and projection M, $\boldsymbol{k}_x$ and $\boldsymbol{k}_y$ are the momenta associated with the Jacobi coordinates $\boldsymbol{x}$ and $\boldsymbol{y}$, s_x and s_y are the coupled spin of the spectator two-body system and the spin of the removed particle, respectively, and σ_x and σ_y are the corresponding spin projections. Finally, $w_{s_x}^{\sigma_x}$ is the continuum two-body wave function of the spectators (^{10}Be and neutron) in the final state. This two-body wave function is computed with the corresponding two-body interaction, and the boundary condition at small distance is determined to be precisely the ^{10}Be-neutron structure left by removing the other neutron in ^{12}Be; see Ref. [60] for a detailed description.

After integration of Eq. (14) over $\boldsymbol{k}_y$ and the angles describing the direction of $\boldsymbol{k}_x$, we obtain the differential cross section $d\sigma/dk_x$, which is related to the invariant mass spectrum as shown in Ref. [36], that is,

$$\frac{d\sigma}{dE_{nc}} = \frac{E_c E_n}{E_c+E_n}\frac{m(M_c+M_n)}{M_c M_n}\frac{1}{k_x}\frac{d\sigma}{dk_x}, \tag{15}$$

where E_c and M_c are the core energy and mass, E_n and M_n the neutron energy and mass, E_{nc} the relative neutron-core energy, and m is the normalization mass used to define the Jacobi coordinates.

The presence in Eq. (14) of the two-body wave function $w_{s_x}^{\sigma_x}(\boldsymbol{k}_x,\boldsymbol{x})$ makes it evident that the invariant mass spectrum (15) crucially depends on the final state two-body interaction. It is important to note that Eq. (14) does not assume that the two spectators populate two-body resonances in the final state. The two-body wave function $w_{s_x}^{\sigma_x}$ contributes to the differential cross section for any value of the relative two-body momentum $\boldsymbol{k}_x$, and not only when $\boldsymbol{k}_x$ matches a two-body resonance energy. Except for those very precise values of $\boldsymbol{k}_x$, $w_{s_x}^{\sigma_x}$ is just an ordinary continuum two-body wave function.

In Fig. 7, we show the relative core-neutron energy spectrum after removal of one neutron from ^{12}Be on a light target according to Eq. (15). The results for the different ^{10}Be-neutron interactions used in this work are shown. The computed curves have been scaled to the experimental data [13]. Also, the experimental energy resolution has been taken into account by convoluting the computed distributions with a Gaussian having a full width at half maximum (FWHM) equal to $0.4E^{1/2}$ (E in MeV) [13].

As a general result, all the potentials reproduce equally well the peak at about 1.2 MeV and the tail of the distribution. In the same way, all of them underestimate the spectrum in the region around 2.2 MeV and do not reproduce the very narrow peak at very low energies. Potential IV reproduces the peak at 1.2 MeV best of all but, on the other hand, gives a worse agreement with the experiment in the region between 3 and 4 MeV. Compared with the results with potential I, the inclusion of the Argonne nucleon-nucleon potential slightly improves the behavior at small energies but also slightly spoils the agreement with the experiment at large energies.

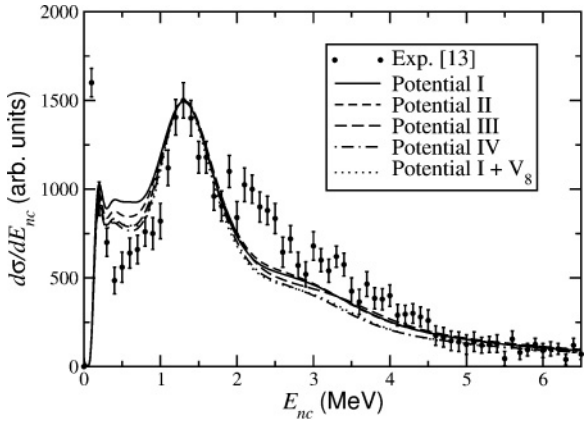

FIG. 7. Relative energy spectrum of ^{10}Be+neutron after fragmentation of ^{12}Be on a light target, obtained by calculations using potentials I–IV and I+v_8. The experimental data correspond to fragmentation of ^{12}Be on carbon at a beam energy of 39.3 MeV/nucleon [13].

In Fig. 8 we show, for different ^{10}Be-neutron potentials, the contributions from s, p, and d waves to the total invariant mass spectrum. Here s, p, and d refer to the value of the ^{10}Be-neutron relative orbital angular momentum. Contributions from the $d_{3/2}$ and $d_{5/2}$ waves are also shown. We notice that the main peak in the distribution is produced by the $d_{5/2}$ wave. This can be traced back to the $5/2^+$ resonance in ^{11}Be at 1.28 MeV above threshold. The $3/2^+$ resonance, with an energy of 2.90 MeV, helps to match the experimental tail of the distribution. The s and p waves contribute mainly at small energies, and they are almost entirely responsible for the distribution below 1 MeV.

From Fig. 8 it is now easy to understand that the main disagreement between the computed curves and the experimental data is due to the absence in the calculation of the $3/2^-$ resonance in ^{11}Be, whose energy above threshold is 2.19 MeV, precisely the energy region where the disagreement is found. However, as already mentioned, inclusion of this resonance necessarily requires information beyond the present ^{12}Be three-body model with an inert ^{10}Be core. If we still insist on the picture of a three-body system with a ^{10}Be core, then a $3/2^-$ state in ^{11}Be needs either a neutron in the p shell coupled to the 2^+ state of ^{10}Be, or a neutron in the sd shell coupled to ^{10}Be in a negative-parity state. Another possibility is of course to use a different cluster description for ^{12}Be, as for instance ^{9}Be in the $3/2^-$ ground state plus three neutrons. Therefore, except for the lack of this state in the ^{11}Be spectrum, the contributions obtained in this work for the 0^+ ground state are consistent with the experimental invariant mass spectrum given in Ref. [13].

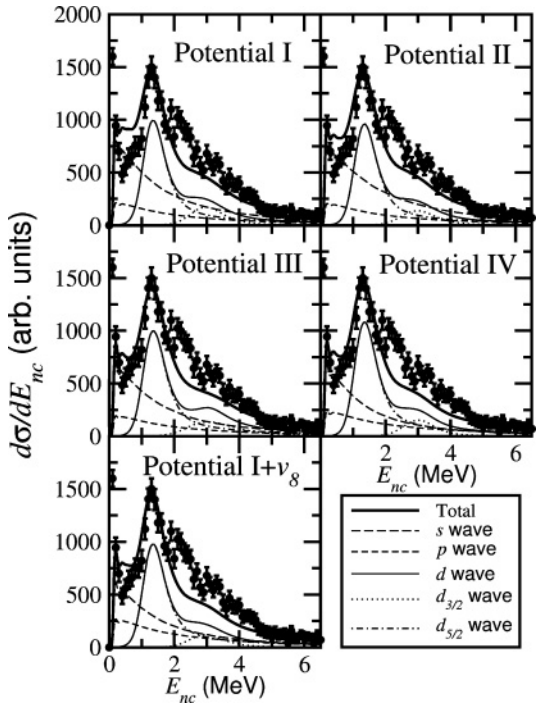

FIG. 8. Relative energy spectrum of ^{10}Be+neutron after fragmentation of ^{12}Be on a light target (thick solid curve), and the contributions to it from s, p, and d waves. The d-wave contribution is split into the $d_{3/2}$ and $d_{5/2}$ contributions. The different panels show the spectra corresponding to the potentials in Table I and the case with potential I plus the Argonne v_8 nucleon-nucleon potential. Experimental data are from Ref. [13].

The highest ^{11}Be resonance that has been considered in our calculations is the $3/2^+$ state at 2.90 MeV. The next excited states in ^{11}Be are the $5/2^-$ and $3/2^-$ resonances with energies above threshold at 3.49 and 3.46 MeV, respectively [52]. For the same reason as the $3/2^-$ state at 2.19 MeV, these two states cannot be included in our three-body picture with an inert ^{10}Be core. In any case, decay of these two resonances into the ground state of ^{10}Be plus a neutron would give some small contribution to the tail of the invariant mass spectrum. However, these two states can also decay into ^{10}Be plus a neutron but leaving ^{10}Be in its 2^+ excited state at 3.37 MeV. Therefore very little energy is left for the neutron after such decay (less than 100 keV [52]), giving rise to the experimental sharp peak at very low energies. Theoretical calculation of this peak requires then also the inclusion of core excitations in the model.

In Ref. [61], the experimental FWHM of the ^{10}Be longitudinal momentum distribution after fragmentation of ^{12}Be on a carbon target (beam energy equal to 56.8 MeV/nucleon) is found to be 194 ± 9 MeV/c. Within the sudden approximation, such distribution can also be computed from Eq. (14), see Ref. [60] for details. The widths of the longitudinal core momentum distributions are computed to be 162, 159, 169, 171, and 166 MeV/c for the neutron-core potentials I, II, III, IV, and I+v_8, respectively.

Inclusion of core excitations should help reduce the discrepancy between the computed widths and the experimental value. The components having spin of the core equal to 2, and coupling to the total angular momentum zero of the ^{12}Be ground state, must necessarily contain nonzero values for ℓ_x or/and ℓ_y. This means the addition of centrifugal barriers that attempt to confine the three-body system to smaller spatial extension, subsequently producing broader momentum distributions.

VII. SUMMARY AND CONCLUSIONS

The properties of ^{12}Be have been investigated assuming a three-body structure with an inert ^{10}Be core and two neutrons. A description of the nucleus by use of the hyperspherical adiabatic expansion method is particularly appropriate in this case, since two of the two-body subsystems have bound states. The symmetric treatment of all the two-body interactions makes it easier to reproduce the correct two-body asymptotics. This could be especially important for the weakly bound excited states.

We constructed four different neutron-^{10}Be interactions, each of them reproducing the known spectrum of ^{11}Be up to an excitation energy of 3.41 MeV. However, the $3/2^-$ resonance in ^{11}Be has been excluded, since it requires the ^{10}Be core to be in an excited state. This case goes beyond the three-body model with an inert core that is used in this work. Nevertheless, part of the effects arising from core deformation are effectively taken into account through the fitting procedure of the neutron-^{10}Be potential. For the neutron-neutron interaction, two different potentials have been used, both reproducing low-energy scattering data.

We have found two 0^+, one 2^+, one 1^-, and one 0^- bound states. The first four are known experimentally, but the 0^- state is not. The computed binding energies agree reasonably well with the experimental value for the ground 0^+ state and the excited 1^- state. For the second 0^+ and the 2^+ states, a larger discrepancy is found, which can be attributed to contributions from core excitations additional to the ones masked in the neutron-^{10}Be potential. To reproduce the experimental two-neutron separation energies for these states, we included a three-body force.

The dominating components of the wave functions correspond to the ones expected from the extreme single-particle model. The ratio of the computed neutron-neutron and core-neutron rms distances increases with the excitation energy. All possible electric and magnetic transition strengths have also been computed. An effective charge for the neutron is used to take into account distortion or polarization of the core. This effective charge has been obtained by adjusting the calculation to reproduce the experimental $\mathcal{B}(E1)$ transition strength in ^{11}Be, as well as its charge rms radius.

Core excitations can contribute to transition strengths in two different ways. There could be a direct contribution arriving from the transition between two core states or a contribution to the wave function of a ^{12}Be state then leading to an indirect effect on transition strengths.

The direct contribution of core excitations in the ^{12}Be monopole and dipole strength functions should be negligible, since r^2, $\mathcal{M}_\mu(E1)$, and $\mathcal{M}_\mu(M1)$ operators cannot couple the $J = 0$ and $J = 2$ states. On the other hand, quadrupole

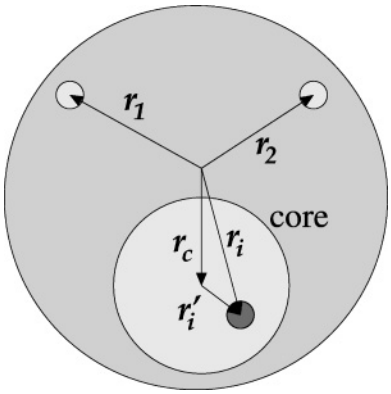

FIG. 9. Coordinates used to calculate the $\mathcal{M}_\mu(E\lambda)$ operator in ^{12}Be three-body cluster. $\boldsymbol{r}_1, \boldsymbol{r}_2$, and $\boldsymbol{r}_c$ give the positions of the three components relative to the center of mass of the system. The coordinate of particle i inside the core is written as $\boldsymbol{r}_i = \boldsymbol{r}_c + \boldsymbol{r}'_i$, where $\boldsymbol{r}'_i$ is its position relative to the core center of mass.

transition operators can couple these states, and there could be an important effect from the excitation of the core. The possible contribution of core excitations to wave functions of 2^+ and 0^+_2 states could lead to some uncertainties in the calculated transition strengths involving those states. Our calculations reproduce rather well the available experimental data.

The relative ^{10}Be-neutron energy spectrum after ^{12}Be breakup on a carbon target at a beam energy of 39.3 MeV/nucleon has been computed within the sudden approximation. For all the potentials, the experimental spectrum is rather well reproduced. Only in the region around 2.2 MeV do the computed curves underestimate the experiment. This is due to the absence of the $3/2^-$ resonance in our ^{11}Be spectrum, which originates from ^{10}Be-core excited states.

In summary, a frozen-core three-body model is able to reproduce most of the properties of ^{12}Be: ground and excited bound states, electromagnetic transition strengths, and invariant mass spectrum after high-energy breakup. Core excitations, however, are needed to improve the two-neutron separation energies for the 0^+_2 and 2^+ states, to obtain a better estimate of the quadrupole transition strengths and monopole transition matrix element, and to fine tune the agreement with the experimental invariant mass spectrum.

ACKNOWLEDGMENTS

We are grateful to K. Riisager for drawing our attention to the problems of weakly bound excited states investigated here. This work was partly supported by the DGI of MEC (Spain) under Contract No. FIS2005-00640. One of us (C.R.R.) acknowledges support by a grant from CSIC and the European Social Fund.

APPENDIX: TRANSITION STRENGTH OPERATORS

For a system made of A constituents, the electric transition operator of order λ, $\mathcal{M}_\mu(E\lambda)$, is defined as

$$\mathcal{M}_\mu(E\lambda) = e\sum_{i=1}^{A} Z_i r_i^\lambda Y_{\lambda,\mu}(\hat{r}_i), \tag{A1}$$

where Z_i is the charge (in units of e) of constituent i, and $\boldsymbol{r}_i$ is its position from the A-body center of mass.

For the particular case of ^{12}Be, we are assuming that the system is clustered, showing a three-body structure made by a core (containing $A-2$ nucleons) plus two additional nucleons outside the core. It is then convenient to write the coordinates of the particles inside the core as $\boldsymbol{r}_i = \boldsymbol{r}_c + \boldsymbol{r}'_i$, where $\boldsymbol{r}_c$ gives the position of the core center of mass relative to the A-body center of mass, and $\boldsymbol{r}'_i$ is the coordinate of constituent i in the core relative to the core center of mass (see Fig. 9). The $\mathcal{M}_\mu(E\lambda)$ operator in Eq. (A1) can then be rewritten as

$$\mathcal{M}_\mu(E\lambda) = e\sum_{i=1}^{A-2} Z_i |\boldsymbol{r}_c + \boldsymbol{r}'_i|^\lambda Y_{\lambda,\mu}(\widehat{\boldsymbol{r}_c + \boldsymbol{r}'_i}) + e\sum_{j=1}^{2} Z_j r_j^\lambda Y_{\lambda,\mu}(\hat{r}_j), \tag{A2}$$

where the index i runs over the $A-2$ constituents in the core, and j labels the two external nucleons.

Making use of Eq. (1) in Ref. [62] (see also Ref. [63]) one can easily see that for $\lambda = 1$, one has

$$\mathcal{M}_\mu(E1) = e\sum_{i=1}^{3} Z_i r_i Y_{1,\mu}(\hat{r}_i) + \mathcal{M}_\mu(E1, \text{core}), \tag{A3}$$

where now i runs over the three constituents, Z_i refers to the charge (in units of e) of each of the three constituents, and $\mathcal{M}_\mu(E1, \text{core}) = e\sum_{i=1}^{A-2} Z_i r'_i Y_{1,\mu}(\hat{r}'_i)$ is the electric dipole transition operator of the core.

In the same way, for $\lambda = 2$, one finds

$$\mathcal{M}_\mu(E2) = e\sum_{i=1}^{3} Z_i r_i^2 Y_{2,\mu}(\hat{r}_i) + \mathcal{M}_\mu(E2, \text{core}) + \sum_{m=-1}^{1} f(m,\mu) r_c Y_{1,m}(\hat{r}_c)\mathcal{M}_{\mu-m}(E1, \text{core}), \tag{A4}$$

whose first two terms are analogous to the ones in Eq. (A3). The last term represents a coupling between the intrinsic core dipole operator and the dipole operator associated with the center of mass of the core, while $f(m,\mu)$ is a well-defined function of the indices m and μ.

[1] F. Ajzenberg-Selove, Nucl. Phys. **A248**, 1 (1975).
[2] F. C. Barker and G. T. Hickey, J. Phys. G **3**, L23 (1977).
[3] L. Johannsen, A. S. Jensen, and P. G. Hansen, Phys. Lett. **B244**, 357 (1990).
[4] I. J. Thompson and M. V. Zhukov, Phys. Rev. C **49**, 1904 (1994).
[5] R. A. Kryger *et al.*, Phys. Rev. C **47**, R2439 (1993).
[6] B. M. Young *et al.*, Phys. Rev. C **49**, 279 (1994).
[7] S. N. Abramovich, B. Ya Guzhovskii, and L. M. Lazarev, Phys. Part. Nuclei **26**, 423 (1995).
[8] M. Zinser *et al.*, Phys. Rev. Lett. **75**, 1719 (1995).

[9] H. B. Jeppesen *et al*., Phys. Lett. **B642**, 449 (2006).
[10] F. C. Barker, J. Phys. G **2**, L45 (1976).
[11] H. T. Fortune, G.-B. Liu, and D. E. Alburger, Phys. Rev. C **50**, 1355 (1994).
[12] A. Navin *et al*., Phys. Rev. Lett. **85**, 266 (2000).
[13] S. D. Pain *et al*., Phys. Rev. Lett. **96**, 032502 (2006).
[14] E. Garrido, D. V. Fedorov, and A. S. Jensen, Nucl. Phys. **A700**, 117 (2002).
[15] M. Zinser *et al*., Nucl. Phys. **A619**, 151 (1997).
[16] M. V. Zhukov, B. V. Danilin, D. V. Fedorov, J. M. Bang, I. J. Thompson, and J. S. Vaagen, Phys. Rep. **231**, 151 (1993).
[17] E. Garrido, D. V. Fedorov, and A. S. Jensen, Nucl. Phys. **A695**, 109 (2001).
[18] M. Fukuda *et al*., Phys. Lett. **B268**, 339 (1991).
[19] R. Anne *et al*., Phys. Lett. **B304**, 55 (1993).
[20] J. H. Kelley *et al*., Phys. Rev. Lett. **74**, 30 (1995).
[21] W. D. Teeters and D. Kurath, Nucl. Phys. **A275**, 61 (1977).
[22] T. Otsuka, N. Fukunishi, and H. Sagawa, Phys. Rev. Lett. **70**, 1385 (1993).
[23] H. Esbensen, B. A. Brown, and H. Sagawa, Phys. Rev. C **51**, 1274 (1995).
[24] P. Descouvemont, Nucl. Phys. **A615**, 261 (1997).
[25] N. Vinh-Mau, Nucl. Phys. **A592**, 33 (1995).
[26] F. M. Nunes, I. J. Thompson, and R. C. Johnson, Nucl. Phys. **A596**, 171 (1996).
[27] S. Fortier *et al*., Phys. Lett. **B461**, 22 (1999).
[28] J. S. Winfield *et al*., Nucl. Phys. **A683**, 48 (2001).
[29] F. M. Nunes, J. A. Christley, I. J. Thompson, R. C. Johnson, and V. D. Efros, Nucl. Phys. **A609**, 43 (1996).
[30] D. E. Alburger, D. P. Balamuth, J. M. Lind, L. Mulligan, K. C. Young, R.W. Zurmuhle, and R. Middleton, Phys. Rev. C **17**, 1525 (1978).
[31] H. Iwasaki *et al*., Phys. Lett. **B481**, 7 (2000).
[32] H. Iwasaki *et al*., Phys. Lett. **B491**, 8 (2000).
[33] S. Shimoura *et al*., Proc. third Int. Conf. on "Exotic Nuclei and Atomic Masses," ENAM 2001, Hameenlinna, Finland, Springer-Verlag 2003, p.339.
[34] S. Shimoura *et al*., Phys. Lett. **B560**, 31 (2003).
[35] F. M. Nunes, I. J. Thompson, and J. A. Tostevin, Nucl. Phys. **A703**, 593 (2002).
[36] E. Garrido, D. V. Fedorov, and A. S. Jensen, Nucl. Phys. **A617**, 153 (1997).
[37] E. Garrido, D. V. Fedorov, and A. S. Jensen, Phys. Rev. C **59**, 1272 (1999).
[38] B. V. Danilin, I. J. Thompson, J. S. Vaagen, and M. V. Zhukov, Nucl. Phys. **A632**, 383 (1998).
[39] E. Nielsen, D. V. Fedorov, A. S. Jensen, and E. Garrido, Phys. Rep. **347**, 373 (2001).
[40] S. Shimoura *et al*., Phys. Lett. **B654**, 87 (2007).
[41] E. Garrido, D. V. Fedorov, and A. S. Jensen, Phys. Rev. C **69**, 024002 (2004).
[42] R. B. Wiringa, V. G. J. Stoks, and R. Schiavilla, Phys. Rev. C **51**, 38 (1995).
[43] F. Ajzenberg-Selove, Nucl. Phys. **A506**, 1 (1990).
[44] G.-B. Liu and H. T. Fortune, Phys. Rev. C **42**, 167 (1990).
[45] D. J. Millener, Nucl. Phys. **A693**, 394 (2001).
[46] N. Fukuda *et al*., Phys. Rev. C **70**, 054606 (2004).
[47] F. Ajzenberg-Selove, Nucl. Phys. **A490**, 1 (1988).
[48] I. Tanihata, T. Kobayashi, O. Yamakawa, K. Sugimoto, N. Takahashi, T. Shimoda, and H. Sato, Phys. Lett. **B206**, 592 (1988).
[49] E. Garrido, D. V. Fedorov, and A. S. Jensen, Nucl. Phys. **A650**, 247 (1999).
[50] D. J. Morrissey *et al*., Nucl. Phys. **A627**, 222 (1997).
[51] H. O. U. Fynbo *et al*., Nucl. Phys. **A736**, 39 (2004).
[52] Y. Hirayama, T. Shimoda, H. Izumi, A. Hatakeyama, K. P. Jackson, C. D. P. Levy, H. Miyatake, M. Yagi, and H. Yano, Phys. Lett. **B611**, 239 (2005).
[53] C. Romero-Redondo, E. Garrido, D. V. Fedorov, and A. S. Jensen, Phys. Lett. **B660**, 32 (2008).
[54] D. J. Millener, J. W. Olness, E. K. Warburton, and S. S. Hanna, Phys. Rev. C **28**, 497 (1983).
[55] Y. Suzuki, H. Matsumura, and B. Abu-Ibrahim, Phys. Rev. C **70**, 051302(R) (2004).
[56] W. Horiuchi and Y. Suzuki, Phys. Rev. C **73**, 037304 (2006).
[57] S. Raman, C. H. Malarkey, W. T. Milner, C. W. Nestor Jr., and P. H. Stelson, At. Data Nucl. Data Tables **36**, 1 (1987).
[58] Y. Kanada-Enyo and H. Horiuchi, Phys. Rev. C **68**, 014319 (2003).
[59] A. Bohr and B. R. Mottelson, *Nuclear Structure*, Vols. 1 and 2 (Benjamin, Reading, MA, 1969, 1975).
[60] E. Garrido, D. V. Fedorov, and A. S. Jensen, Phys. Rev. C **55**, 1327 (1997).
[61] M. Zahar *et al*., Phys. Rev. C **48**, R1484 (1993).
[62] J. M. Dixon and R. Lacroix, J. Phys. A **6**, 1119 (1973).
[63] J. M. Dixon and R. Lacroix, J. Phys. A **7**, 552 (1974).